Geophysical Research Letters

RESEARCH LETTER
10.1002/2017GL076417

Key Points:
- Coseismic surface deformation of the 2017 Mw 6.5 Ormoc earthquake measured by multisight InSAR data along a creeping segment of the Philippine Fault
- Ascending, descending InSAR displacements, and SAR azimuth offset displacements help infer coseismic fault geometry and slip model
- The slip deficit underneath the Tongonan geothermal field suggests that high geothermal gradient could prevent the coseismic failure

Supporting Information:
- Supporting Information S1

Correspondence to:
J.-C. Hu,
jchu@ntu.edu.tw

Citation:
Yang, Y.-H., Tsai, M.-C., Hu, J.-C., Aurelio, M. A., Hashimoto, M., Escudero, J. A. P., et al. (2018). Coseismic slip deficit of the 2017 Mw 6.5 Ormoc earthquake that occurred along a creeping segment and geothermal field of the Philippine Fault. *Geophysical Research Letters*, *45*, 2659–2668. https://doi.org/10.1002/2017GL076417

Received 20 NOV 2017
Accepted 9 MAR 2018
Accepted article online 15 MAR 2018
Published online 25 MAR 2018

Coseismic Slip Deficit of the 2017 Mw 6.5 Ormoc Earthquake That Occurred Along a Creeping Segment and Geothermal Field of the Philippine Fault

Ying-Hui Yang[1,2], Min-Chien Tsai[3], Jyr-Ching Hu[2], Mario A. Aurelio[4], Manabu Hashimoto[5], John Agustin P. Escudero[4], Zhe Su[6], and Qiang Chen[7]

[1]School of Civil Engineering and Architecture, Southwest Petroleum University, Chengdu, China, [2]Department of Geosciences, National Taiwan University, Taipei, Taiwan, [3]Seismological Center, Central Weather Bureau, Taipei, Taiwan, [4]National Institute of Geological Sciences, University of the Philippines, Quezon City, Philippines, [5]Disaster Prevention Research Institute, Kyoto University, Kyoto, Japan, [6]Key Laboratory of Crustal Dynamics, Institute of Crustal Dynamics, China Earthquake Administration, Beijing, China, [7]Department of Remote Sensing and Geoinformation Engineering, Southwest Jiaotong University, Chengdu, China

Abstract Coseismic surface deformation imaged through interferometric synthetic aperture radar (InSAR) measurements was used to estimate the fault geometry and slip distribution of the 2017 Mw 6.5 Ormoc earthquake along a creeping segment of the Philippine Fault on Leyte Island. Our best fitting faulting model suggests that the coseismic rupture occurred on a fault plane with high dip angle of 78.5° and strike angle of 325.8°, and the estimated maximum fault slip of 2.3 m is located at 6.5 km east-northeast of the town of Kananga. The recognized insignificant slip in the Tongonan geothermal field zone implies that the plastic behavior caused by high geothermal gradient underneath the Tongonan geothermal field could prevent the coseismic failure in heated rock mass in this zone. The predicted Coulomb failure stress change shows that a significant positive Coulomb failure stress change occurred along the SE segment of central Philippine Fault with insignificant coseismic slip and infrequent aftershocks, which suggests an increasing risk for future seismic hazard.

Plain Language Summary A shallow earthquake with magnitude 6.5 hit northern sector of Leyte Island along the Philippine Fault near the Tongonan geothermal field. This earthquake resulted in at least 4 fatalities and 100 injuries. The seismicity is not frequent, and no large earthquake has been reported on Leyte Island since the 17th century. As a result, this earthquake will increase the risk of seismic hazard on the surrounding fault system. Thus, the detailed investigation on the activity of the fault on Leyte Island is a crucial issue for earth scientist and governmental agency.

1. Introduction

On 6 July 2017, an Mw 6.5 earthquake struck the northern sector of Leyte Island in the central Philippines, with the epicenter located about 6.5 km north-northeast of Ormoc City in a region underlain by an active geothermal system. A shallow earthquake source depth resulted in strong surface shaking and significant seismic damage that caused at least 4 fatalities and 100 injuries. This event occurred along the central segment of the Philippine Fault that traverses Leyte Island, leaving a surface rupture in the vicinity of the town of Kananga. The Philippine Fault is a 1,200 km-long sinistral fault resulting from the partitioning of the oblique convergence between the Philippine Sea Plate and Eurasia (Figure 1) (Aurelio, 2000; Barrier et al., 1991; Besana & Ando, 2005). This mechanism was first proposed by Fitch (1972) and later adopted by other workers to explain the existence of other large strike-slip faults behind oblique convergence zones such as the Karakoram fault system in Kashmir Himalaya (Kundu et al., 2014), the Variscan fault in the SW Iberian (Pérez-Cáceres et al., 2015), the Great Sumatran Fault in Indonesia (Maung, 1987; McCaffrey et al., 2000), the Median Tectonic Line in Japan (Taira et al., 1983), the Alpine Fault in New Zealand (Claypool et al., 2002; Walcott, 1998), and the Ramu-Markham Fault in Papua New Guinea (Dow & Sukamto, 1984). In this mechanism, the PSP-Eurasia oblique convergence of about 9.8 cm/yr (DeMets et al., 2010) is decomposed into two components, namely, (1) a frontal subduction perpendicular to the axis of the Philippine Trench and (2) a sinistral slip accommodated along the NW-SE trending Philippine Fault (Figure 1). The partitioning is also responsible for the northwest dispersion of tectonic blocks within the Philippine Mobile Belt, well

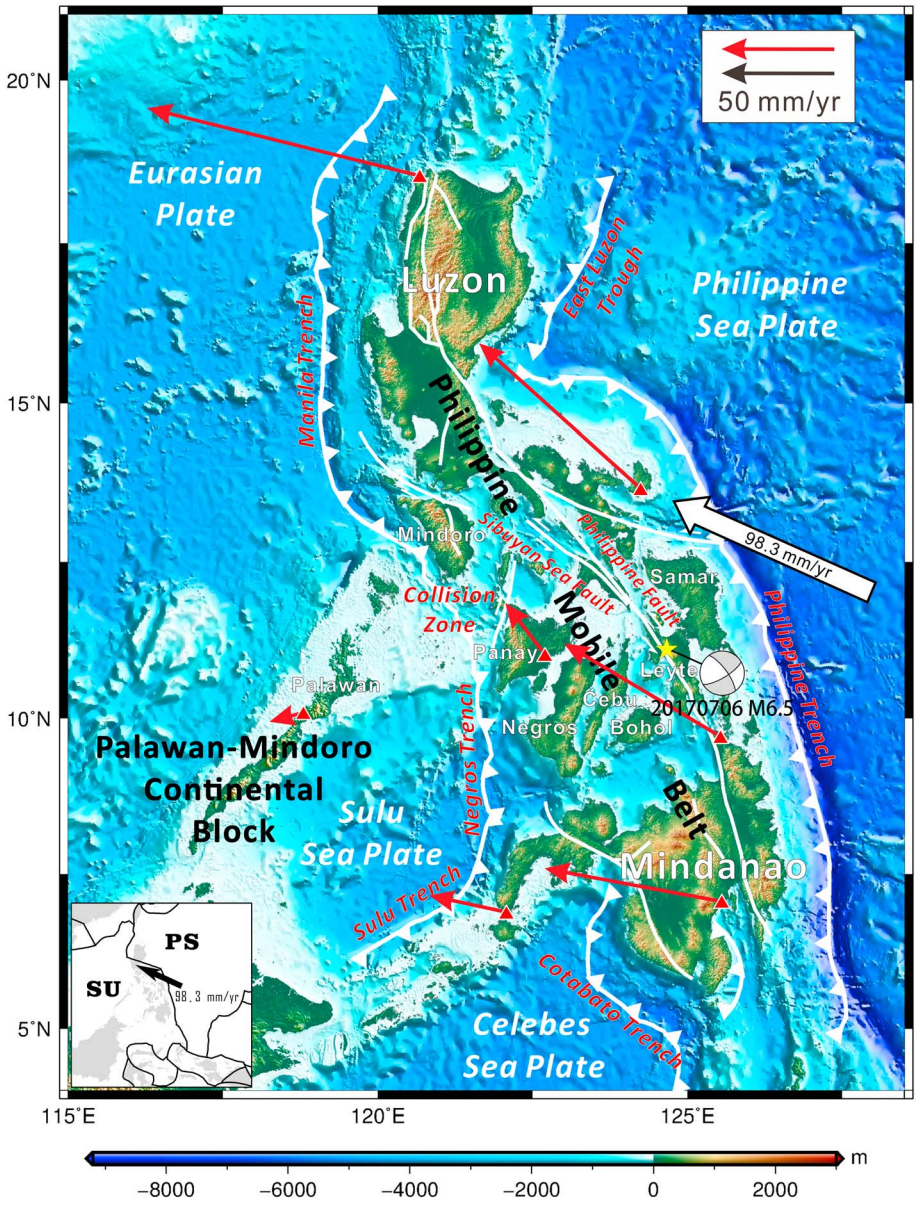

Figure 1. Tectonic setting of the Philippines characterized by opposing subduction systems and a major sinistral fault: The Philippine Fault System. The map also shows NW directed block motion vectors (red arrows) from GEODYnamics of south and SE Asia (Aurelio et al., 1998). The sinistral Philippine Fault is a consequence of the partitioning of oblique convergence (white arrow from DeMets et al., 2010) between the Philippine Sea Plate and Eurasia. See text for more discussion.

detected in recent Global Positioning System (GPS) measurements (Aurelio et al., 1998; Bacolcol, 2003; Becker et al., 1998; Kreemer et al., 2000; Rangin et al., 1999).

Previous studies show that the seismic activity along the Philippine Fault zone is frequent but not uniform (Duquesnoy et al., 1994; Prioul et al., 2000). Since 1860, about 10 events with magnitude larger than Ms 7.0 have occurred along segments in the major islands of Luzon, Visayas, and Mindanao. On the other hand, no large event has been reported on Leyte Island since the 17th century, with only low-magnitude seismicity being generated along the Leyte segment of the Philippine Fault. This phenomenon is attributed to a creeping motion of the Leyte segment based on the large shear displacement rate of around 2.6 cm/yr detected by GPS campaigns across the fault trace (Duquesnoy et al., 1994). The previous studies based on geodetic investigations demonstrated that the average creeping rate in northern Leyte segment near the seismogenic zone of Ormoc event is about 3.5 cm/yr (Bacolcol, 2003; Prioul et al., 2000).

In addition, it has been suggesting that the fault creeping motion may be controlled by the thermal structure of the upper crust of Leyte Island revealed by the induced seismicity experiment across the creeping fault near the Tongonan geothermal field (Prioul et al., 2000). The 2017 Mw 6.5 Ormoc earthquake is the largest seismic event striking the Leyte Island in the last 400 years. The focal mechanism of the main shock is mainly NW striking sinistral strike-slip type with minor normal component dipping to the NE. This is consistent with the geological observation (e.g., Aurelio, 1992) for the western branch of the Philippine Fault as a NNW striking and NE dipping strike-slip fault (Figure 1). In general, the location and focal mechanism of major aftershock coincides very well with a steep sinistral strike-slip fault with minor normal component to the SE. In Leyte, the NW striking Philippine Fault splits into two main branches: a west branch dipping to the NE and an east branch dipping to the SW (Figure S1 in the supporting information). These two branches form a sinistral-normal duplex (negative flower structures) that displaces a stratovolcano called Mt. Bao, which is the host of the Tongonan Geothermal field, the largest producing geothermal plant in the Philippines (Aurelio et al., 1993). In addition, the occurrence of the Ormoc event indicates that the creeping rate along the Leyte segment is not uniform, the strain has been accumulated at the low creeping rate of the northern Leyte segment, and the accumulated strain energy resulted in this earthquake event.

Field observations and the dense shallow aftershocks with source depths less than 3 km suggest that the fault rupture could propagate to the ground surface (Philippine Institute of Volcanology and Seismology, 2017). However, the coseismic fault geometry, slip distribution, and the associated stress change of the Ormoc event are not well known so far. Interferometric synthetic aperture radar (InSAR) technique can resolve coseismic surface deformation with a resolution high enough to estimate the coseismic source model (Chen et al., 2015; Huang et al., 2016; Massonnet et al., 1993; Yang et al., 2014). Both of ALOS-2 and Sentinel-1A satellites have captured the synthetic aperture radar (SAR) images before and after the Ormoc earthquake. In this paper, we jointly use the SAR images of ALOS-2 and Sentinel-1A to infer the fault geometry and coseismic slip model of the 2017 Ormoc earthquake. The estimated source model is then used to determine the Coulomb stress change in and around this seismogenic fault, which provides the valuable assessment for the future seismic hazard.

2. Data Sets and InSAR Measurements

We combined the ascending, descending tracks data of ALOS-2 and Sentinel-1A (S1A) satellites for measuring the coseismic surface deformation field to estimate the fault geometry and slip model associated with the Ormoc event. Table S1 shows the main parameters of the used ALOS-2 and Sentinel-1A images, and all of the three tracks cover the entire seismic area (Figure 2).

Both ascending and descending tracks ALOS-2 L-band SAR images, acquired in the strip-map mode, were processed using the GMTSAR software with a multilook factor of 32 × 12 (azimuth multifactor × range multilook factor) to maintain the interferometric correlation in the near-fault zone (Sandwell et al., 2011; Yang et al., 2013). The SRTM-4 digital elevation model was used to remove the topographic contribution from the initial interferogram. The unwrapped phase data were detrended by removing the 2-D ramp estimated from the far-field data with high coherence to account for orbital errors (Chen & Zebker, 2002). As shown in Figures 3a and 3b, the ALOS-2 tracks maintain excellent interferometric coherence in the nearfield of fault zone, and dense fringes have been acquired around the seismogenic fault in the interferograms both on the ascending and descending tracks. Two Sentinel-1A C-band SAR images along descending track, acquired in the TOPS (Terrain Observation with Progressive Scan) imaging mode, were processed by the GAMMA InSAR software with a multilook factor of 20 × 6 (Wegmuller & Werner, 1997). Figure 3c shows the S1A interferogram around the seismogenic fault, and the far-field S1A data have been removed due to slight coseismic surface movement but significant atmospheric delay signal. As shown in Figure 3c, the coseismic surface deformation in near-fault zone is not effectively observed due to the interferometric decorrelation caused by large phase gradient and dense vegetation.

We get the Azimuth Offset (AO) displacement fields of ALOS-2 descending track using offset-tracking technique (Michel et al., 1999; Yang, Chen, Xu, Zhang, Yong, & Liu, 2017); the result is shown in Figure 3d. Both InSAR interferograms and AO displacement field show that there are two significant deformation quadrants over the northwest portion of the Leyte fault zone. Furthermore, the discontinuities of InSAR phases and AO displacements can be found near the surface trace of north Leyte fault, which suggests that the fault

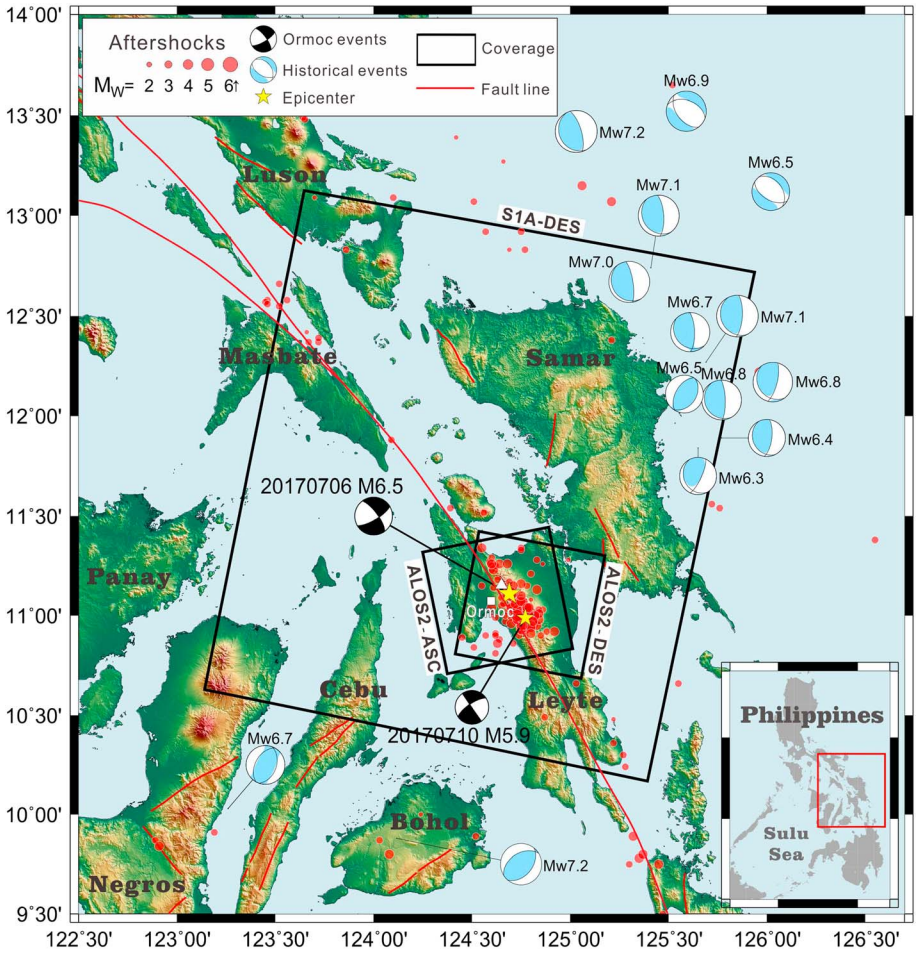

Figure 2. Ground coverage of used ALOS-2 and Sentinel-1A SAR images. Central Philippine Faults (the red lines) and aftershocks (the red circles) are mapped on a shaded relief of SRTM-4 digital elevation model. Black dotted rectangles indicate the coverage of ALOS-2 ascending, ALOS-2 descending, and Sentinel-1A descending tracks, respectively. Focal mechanisms of historical events are from Global Centroid Moment Tensor solution.

rupture propagated to the ground surface. Moreover, considering the strike of northwest segment of Leyte fault is nearly parallel to the flight direction of ascending track of ALOS-2, and the InSAR trough-to-peak displacements along ascending track are smaller than those along the descending track; we infer that the Mw 6.5 Ormoc earthquake may have been caused by an east dipping fault with a dominated left-lateral strike slip.

3. Method of Inversion of Fault Model

The coseismic InSAR data are down sampled using a two-dimensional quantization algorithm known as quadtree (Welstead, 1999). Furthermore, the samples with interferometric coherence <0.3 are removed to enhance the quality of used InSAR observations. We preserve totally 4,490 samplings in the coseismic zone (1,862 for ALOS-2 ascending track, 1,681 for ALOS-2 descending track, and 947 for Sentinel-1A descending track). The AO displacement data are not used to estimate the coseismic source model due to low observation accuracy.

Our fault geometry and slip inversion assume that the coseismic rupture occurs on a single planar fault for the main quake. The initial coseismic fault rupture trace is detected based on the AO displacement fields (Yang, Chen, Xu, Zhang, Luo, et al., 2017), which is indicated by the black solid line in Figure 3d. Then we construct a 40 km $\times$ 32 km fault plane and discretize it with a size of 4 km $\times$ 4 km to estimate the fault geometry parameters. The attitude of planar fault geometry is set their bounds of [310°, 350°] for strike, and [50°, 90°] for

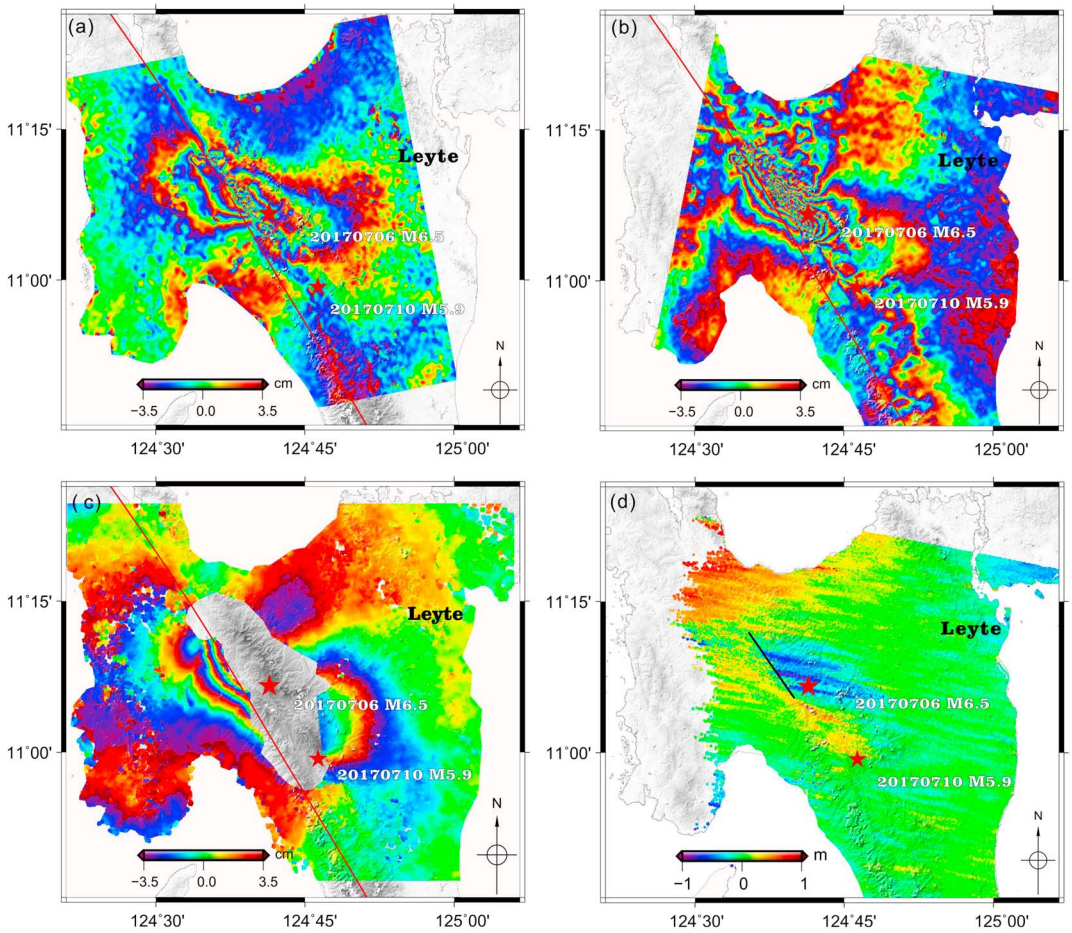

Figure 3. Observed coseismic surface displacements of the Ormoc earthquake revealed interferometric synthetic aperture radar interferograms. (a) ALOS-2 ascending, (b) ALOS-2 descending, and (c) Sentinel-1A descending tracks. (d) Azimuth offset displacements derived from ALOS-2 descending track synthetic aperture radar data. The red stars indicate the location of main shock and the largest aftershock of the Ormoc event. The red lines denote the central Philippine Fault trace on Leyte Island. The black line is the recognized coseismic fault rupture trace from azimuth offset displacement field of the Ormoc event.

dip according to the focal mechanism solution of U.S. Geological Survey (USGS). Laplace smoothing constraints of the adjacent fault patches are applied to avoid the abrupt variations of fault slip. The constraint of no significant slip at the fault edges except at the ground surface is applied to further regularize the inversion problem of fault parameters. The initial inversions are carried out assuming that there are only left-lateral strike slip and normal slip components of the main quake according to the focal mechanism of USGS. However, it is found that the best fitting fault model fails to provide a good fit to ascending and descending tracks InSAR observations simultaneously. We then set the rake angle to vary in the range of [−45°, 45°] and inverse for the fault slip based on assumed fault geometry model.

To optimize the fault geometry and slip parameters, we employ rectangular dislocation in a homogeneous elastic half-space to compute theoretical surface InSAR deformation (Okada, 1985) and compare the data fitting based on its explained ratio, which is defined as follows:

$$\rho = 1 - \sqrt{\frac{\sum (\mathrm{Ob}_i - \mathrm{Pr}_i)^2}{\sum \mathrm{Ob}_i^2}} \tag{1}$$

where Ob_i indicates the InSAR observed data, Pr_i is the predicted data calculated based on the faulting model, and ρ is the explained ratio. The simulated annealing algorithm is used to search the best fitting fault parameters until the globally maximal explained ratio is got. After the best fitting fault geometry parameters are determined, we will rediscretize the fault using the size of 1 km × 1 km with the fixed above geometry parameters to estimate the detailed fault slip distribution.

Table 1
Estimated Fault Parameters of the 2017 Ormoc Earthquake

Parameter	Dip angle (°)	Strike angle (°)	Rake angle (°)
Estimated value	78.5 ± 2.3	325.8 ± 1.7	41.4 ± 3.4

4. Result and Discussion

Table 1 shows the estimated fault parameters and the relative errors. And the optimal rake angle is 41.4° that indicates left-lateral slip with thrust motion of Ormoc earthquake. The joint inversion of multisight InSAR data are solved in a least squares sense based on above best fitting fault parameters (Lawson & Hanson, 1974), thus deriving the fault

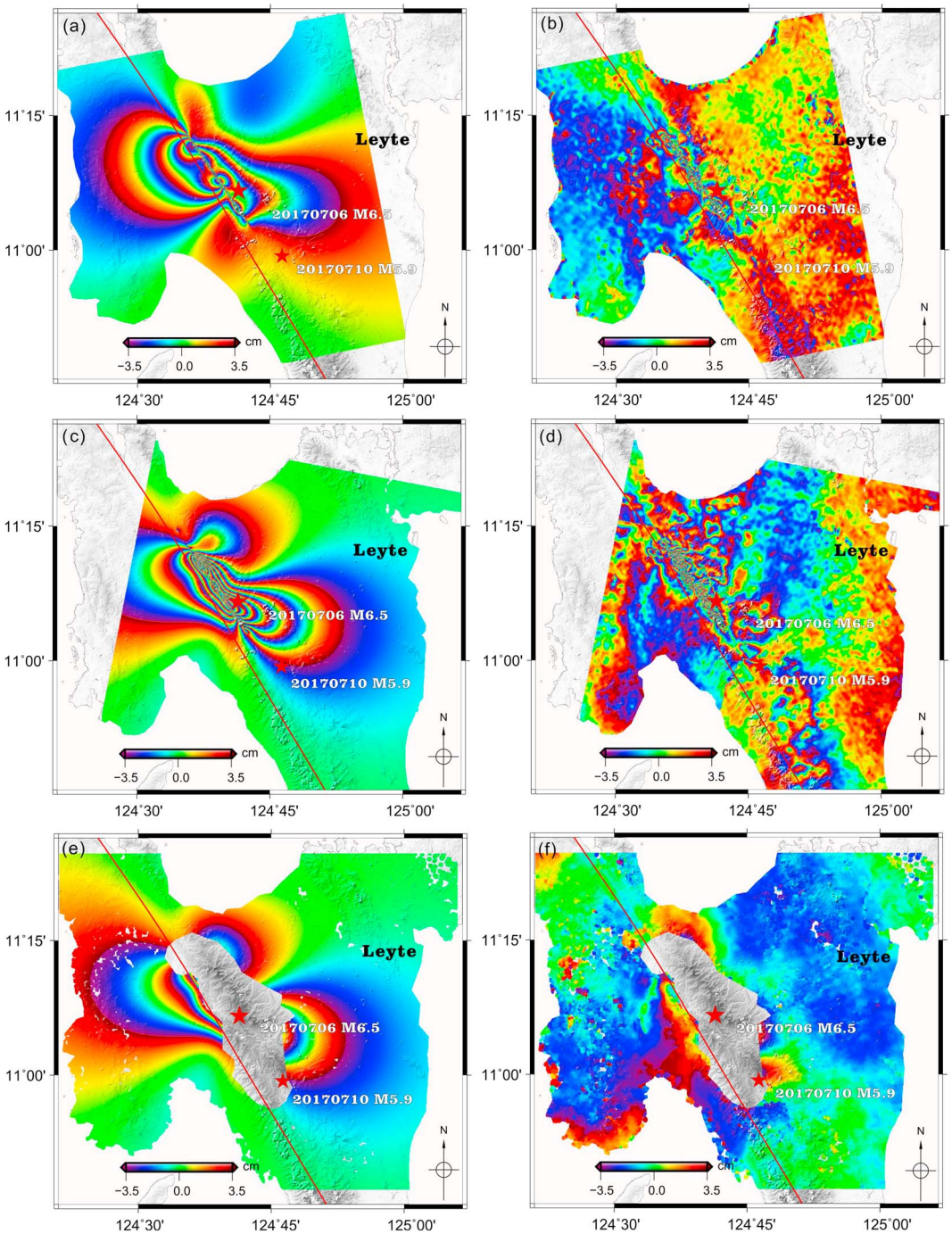

Figure 4. Predicted coseismic surface interferometric synthetic aperture radar (InSAR) displacement field and residual distribution between the observed and predicted deformation. (a) and (b) are from ALOS-2 ascending InSAR. (c) and (d) are from ALOS-2 descending InSAR. (e) and (f) are from Sentinel-1A descending InSAR. Red stars denote the location of main shock and largest aftershock of Ormoc earthquake. Red lines indicate the Philippine Fault trace on Leyte Island.

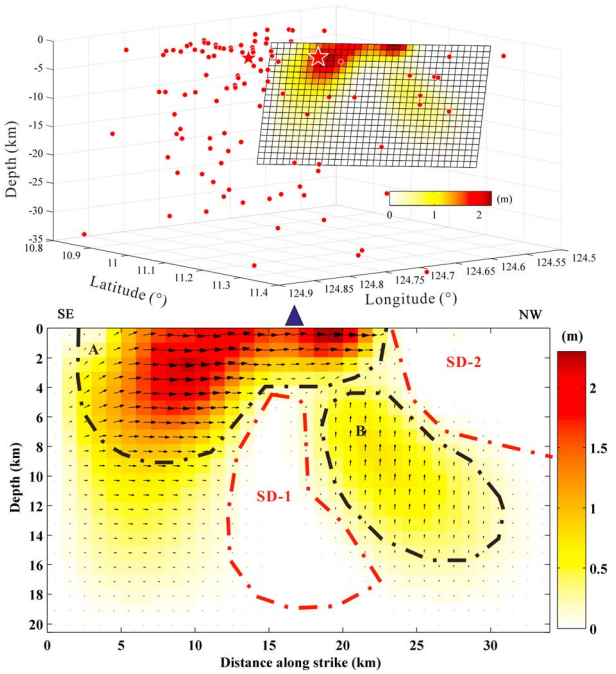

Figure 5. Fault slip model of the Ormoc earthquake. Red solid circles are the aftershocks. Red stars denote the hypocenters of main shock and the largest aftershock with magnitude of M 5.9. Blue triangle indicates the Tongonan Geothermal Power Plant, the black dotted zones indicate the significant coseismic slip concentration, and the red dotted line denotes the slip deficit zone.

slip model, the explained ratios are respectively 86%, 90% for ALOS-2 ascending and descending tracks data, and 93% for Sentinel-1A descending track data. In order to further assess the reliability of the estimated slip model, we forward calculate the InSAR deformation using the derived fault model (Okada, 1985). Figures 4a, 4c, and 4e show the predicted InSAR surface displacements, which are basically consistent with the InSAR observations both of the ascending and descending tracks shown in Figure 3, and the model misfits are 3.9 cm, 3.8 cm, and 3.8 cm for ALOS ascending, descending, and Sentinel-1A descending tracks data, respectively. A few residual fringes of Figures 4b, 4d, and 4f could result from the combined contribution of interferometric decorrelation in near fault, phase unwrapping error, atmospheric delay error, and the surface deformation contributed from aftershocks.

In addition, to evaluate the resolution of our inversion, a checkboard test with the same parameterization of the real inversion is carried out. We firstly simulate a fault model with the same geometry parameters as the inferred fault model of the 2017 Ormoc earthquake. Then a checkboard slip model (see Figure S3a) is considered as the assumed coseismic rupture model, which is used to calculate the synthetic InSAR observations with the same spatial distribution as the real data samples descripted in section 3. And the calculated InSAR data are used to infer the slip distribution, and the result is shown in Figure S3b. It can be found from the comparison between the simulated (Figure S3a) and inferred (Figure S3b) slip models that most of the simulated slip can be recovered both in shape and magnitude, especially for the slip occurred in the shallow crust. Moreover, as expected, we find the phenomenon that the slip resolution is decreasing with the increasing of the depth, which coincides with the previous studies (Cheloni et al., 2017). In general, this checkboard test indicates that the slip distribution can be well resolved, and the inferred slip model of the 2017 Ormoc earthquake by ALOS-2 and Sentinel-1 InSAR observations is reliable.

Figure 5 shows the estimated fault slip model. It suggests that this earthquake is a predominantly left-lateral strike-slip event with minor dip-slip motion. Main fault slip is located at the northwest of the hypocenter, which indicates that the fault rupture propagates from southeast to northwest. Figure 5 shows that the coseismic fault has a length of 35 km, but more than 95% of seismic moment is released in the along-strike distance of 4–22 km from southeastern end of the fault. The fault slip has propagated to the ground surface, and the estimated peak fault slip of 2.3 m locates at 6.5 km northeast of Kananga city. Significant slip is concentrated on the fault patches at depth of 0–10 km and an along-strike distance of 28 km from SE end of the modeled fault with varying slip magnitude from 0.3 m to 2.3 m along the seismogenic fault.

Two significant slip concentrations marked by "A" and "B" can be recognized in Figure 5, which contributes the major surface deformation observed in Figure 3. The area "A" with average slip of 1.5 m is located at depths of 0–9 km and an along-strike distance of 3–24 km from SE end of the fault; it is dominated by left-lateral strike slip with minor thrust and normal slip. The areas "B" with an average slip of 0.4 m is located at depth of 4–16 km and at an along-strike distance of 19–28 km from SE end of the fault; it shows a dominant thrust motion with minor left-lateral strike slip component. Moreover, we found two slip deficit zones underneath of Geothermal field (SD-1) and the northwest portion of the seismogenic fault (SD-2) with insignificant slip and infrequent of aftershocks on the fault plane (Figure 5). Moreover, it can be found from the checkboard test (Figure S3) that the slip can be successfully estimated by the used InSAR observations if there are slips occurred in these two slip deficit zones, which suggests the detected two slip deficit zones are reliable. The seismic moment derived from our preferred slip model is 7.78×10^{18} Nm (equivalent to a moment magnitude of Mw 6.6), which is slight greater than 7.06×10^{18} Nm (Mw 6.5) of the USGS solution, which should result from different observed data (seismic wave data for USGS and InSAR geodetic data for our study) and fault geometry models.

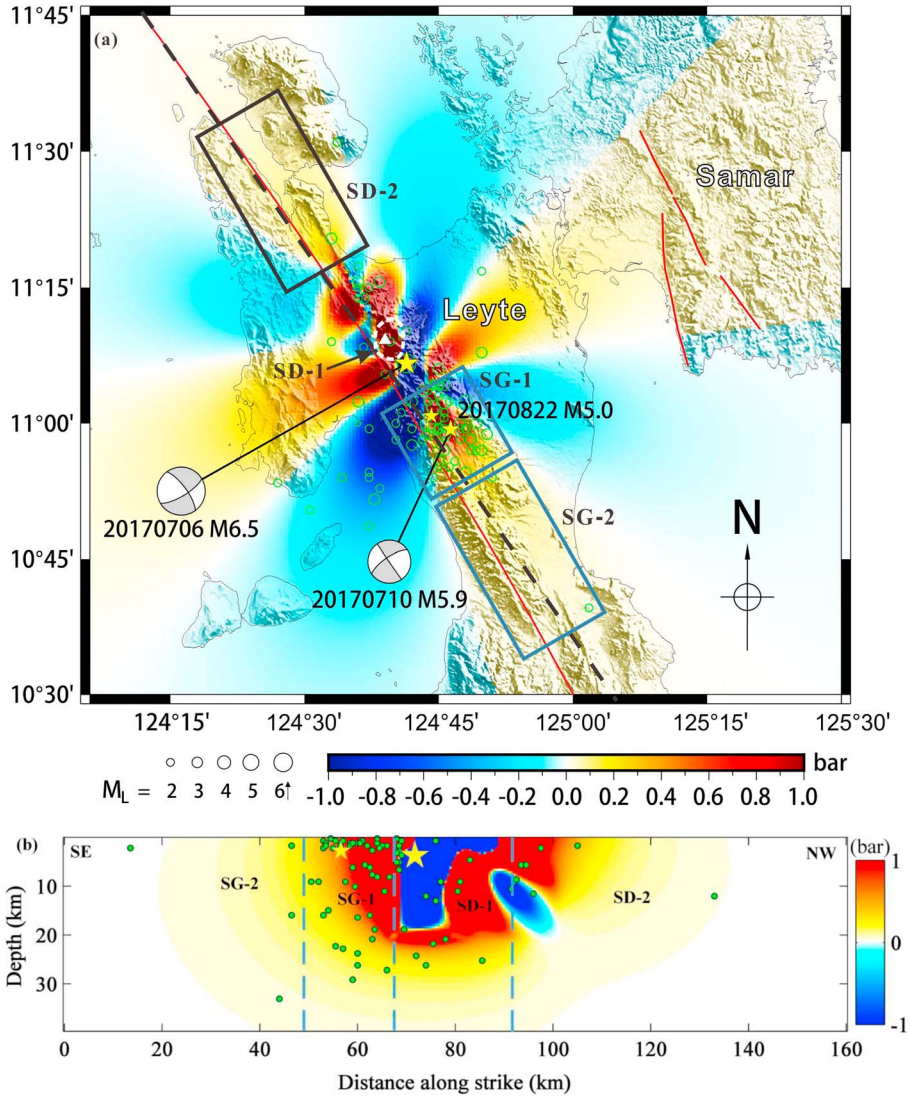

Figure 6. The Coulomb failure stress change at the depth of 6.5 km (a) and along Leyte fault (b). The black dotted line indicates the surface trace of the Coulomb failure stress change section of Figure 6b. The yellow stars denote the location of main shock and largest aftershock of the Ormoc event. The red lines indicate the surface fault traces around Leyte Island, and the polygons denote the zones with significant Coulomb failure stress change. The white line indicates the slip deficit zone of "SD-1", and the white triangle denotes the location of Tongonan Geothermal Power Plant.

Previous studies show that Coulomb failure stress (CFS) change derived from the main shock plays an important role to trigger slip in neighboring seismic zone (Chen et al., 2015; Hanks, 1977). Here we calculate the CFS change at the depth of 6.5 km (Figure 6a) and along the Leyte segment (Figure 6b) based on our preferred coseismic fault model with the receiver fault parameters of 325.8° for strike, 78.5°E for dip, 2.6° for rake, and the friction coefficient of 0.4. Four positive CFS change lobes could be recognized (Figure 6a), and more than ~60% aftershocks occurred in these CFS increasing zones. Figure 5a shows that two small faults located in the eastern Samar Island have positive CFS changes about ~0.1 bar, which enhance the seismic potential if these two fault systems are critically stressed and close to failure.

The recognized slip deficit zone of "SD-1" within the white line in Figure 6 has an average positive CFS change more than ~0.9 bar; it usually indicates high potential of future seismic hazard. However, abundant geothermal source has been found in this zone, and the Tongonan Geothermal Power Plant is located at this zone. The well-injection experiment found that the temperature is higher than ~300° at the depth of 1 to 2 km in this zone (Prioul et al., 2000, see Figure S2). It implies that the predominated plastic deformation of the crustal rock might occur within the high geothermal gradient zone, which prevent the heated rock mass

from fault failure. Therefore, although the positive CFS change is significant, we still believe that there is a low risk of future seismic hazard due to high geothermal gradient in this zone. Figure 6 shows that another recognized slip deficit zone of "SD-2" has an average positive CFS change ~0.6 bar. However, the interseismic creeping motion measured by PS-InSAR technique using the ALSO-1 PALSAR images acquired between 2006 and 2011 shows that a significant interseismic surface motion (~10 mm/yr) has been detected in the segment of "SD-2," which suggests a high creeping rate in this zone. And the accumulated strain energy was released by the high rate interseismic creeping motion, which decreased the risk of fault rupture and resulted in the slip deficit in SD-2 segment. Therefore, we hypothesize that the "SD-2" segment also has a low risk of the future seismic hazard due to high interseismic creeping rate.

The extended segment (marked by "SG-1" in Figure 6) of coseismic fault along southeast direction has significant positive CFS change with an average of ~0.8 bar, which has triggered lots of aftershocks including the largest event with a magnitude of Mw 5.9 in this zone. The average positive CFS change is ~0.2 bar with no aftershocks in "SG-2" segment, and no sufficient evidence suggests significant creeping motion (Figure S4) in this zone. Therefore, it may be a segment with increasing risk of seismic hazard. Moreover, some aftershocks can be found that occurred in the negative lobes of CFS change, which could be considered to be triggered by dynamic Coulomb stress change.

5. Conclusion

This study is a multidisciplinary effort to preliminarily understand the 2017 Mw 6.5 Ormoc earthquake in the context of coseismic surface displacement, faulting mechanism, CFS change, and the seismic hazard. We firstly get multisight cosiesmic surface displacement fields associated with the main shock based on InSAR and offset-tracking technologies. Then, a best fitting fault geometry and slip model are estimated based on the multisight InSAR data. The inferred faulting model demonstrates that the Mw 6.5 Ormoc earthquake ruptures a ~35 × 20 km patch of the Leyte fault in the northeast of Leyte Island. Coseismic fault slip propagated to the ground surface, and the estimated peak fault slip of 2.3 m is located at 6.5 km east-northeast of the Kananga city. The recognized slip deficit zone underneath the Tongonan Geothermal Power Plant could be due to the rock plastic behavior caused by high geothermal gradient in this zone acted as barrier against rupture propagation. The southeast segment of the Leyte fault has significant positive CFS change and low interseismic creeping rate, and absence of aftershocks and main shock slip, which indicates increasing risk of future seismic hazard.

Acknowledgments
The comments of Zhenghong Li and Giuseppe Solaro largely improve this manuscript. This work is supported by the National Key R&D Program of China (2017YFB0502700), the Ministry of Science and Technology in Taiwan under the grants 105-2811-M-002-180 and 106-2116-M-002-004, and the National Natural Science Foundation of China (41472255). ALOS-2 SAR images were provided by the Japan Aerospace Exploration Agency (JAXA) and were processed by the GMTSAR software (Sandwell et al., 2011). Sentinel-1A SAR images were provided by the European Space Agency (ESA) and were processed by the GAMMA software (Wegmuller & Werner, 1997). SRTM DEM data are the void-filled seamless SRTM data V4, available from the CGIAR-CSI SRTM 90 Database: http://srtm.csi.cgiar.org/. Figures were generated using the Generic Mapping Tools (GMT) software (Wessel & Smith, 1998).

References

Aurelio, M. A. (1992). Tectonics of the central segment of the Philippine Fault: Structures, kinematics and geodynamics. (Doctoral Dissertation, T92-T22, 500 pp.). France: Université Pierre et Marie Curie, Memoires des Sciences de la Terre, Academie de Paris.

Aurelio, M. A. (2000). Shear partitioning in an island arc setting: Constraints from Philippine Fault and recent GPS data. *Island Arc*, *9*, 585–598.

Aurelio, M. A., Pagado, E. S., & Tebar, H. J. (1993). Kinematics of the Philippine Fault System at the Tongonan Geothermal Field, N. Leyte: Implications for geothermal exploration and development. *Journal of the Geological Society of the Philippines*, *48*(1–2), 1–20.

Aurelio, M. A., Simons, W. F., Almeda, R. L., & the Philippine GPS Team (1998). Present-day plate motions in the Philippines: Interpretation of GPS results of GEODYSSEA. In P. Wilson & G. Michel (Eds.), *The GEODYnamics of S and SE Asia (GEODYSSEA) Project* (Sci. Tech. Rep. STR98/14, pp. 251–263). Potsdam, Germany: GeoForschungsZentrum.

Bacolcol, T. U. (2003). Geodesic studies of the Philippine Fault in the Visayas. (Doctoral Dissertation, 208 pp.). France: Université Pierre et Marie Curie, Memoires des Sciences de la Terre, Academie de Paris.

Barrier, E., Huchon, P., & Aurelio, M. (1991). Philippine fault: A key for Philippine kinematics. *Geology*, *19*(1), 32–35. https://doi.org/10.1130/0091-7613(1991)019%3C0032:PFAKFP%3E2.3.CO;2

Becker, M., Neumaier, P., Boonphakdee, C., Aurelio, M., Almeda, R., & Kasser, M. (1998). Present-day plate motions in the Philippines: Interpretation of GPS results of GEODYSSEA. In P. Wilson & G. Michel (Eds.), *The GEODYnamics of S and SE Asia (GEODYSSEA) Project* (Sci. Tech. Rep. STR98/14, pp. 162–167). Potsdam, Germany: GeoForschungsZentrum.

Besana, G. M., & Ando, M. (2005). The central Philippine fault zone: Location of great earthquakes, slow events and creep activity. *Earth, Planets and Space*, *57*(10), 987–994. https://doi.org/10.1186/BF03351877

Cheloni, D., De Novellis, V., Albano, M., Antonioli, A., Anzidei, M., Atzori, S., et al. (2017). Geodetic model of the 2016 Central Italy earthquake sequence inferred from InSAR and GPS data. *Geophysical Research Letters*, *44*, 6778–6787. https://doi.org/10.1002/2017GL073580

Chen, C. W., & Zebker, H. A. (2002). Phase unwrapping for large SAR interferograms: Statistical segmentation and generalized network models. *IEEE Transactions on Geoscience and Remote Sensing*, *40*(8), 1709–1719. https://doi.org/10.1109/TGRS.2002.802453

Chen, Q., Yang, Y., Luo, R., Liu, G., & Zhang, K. (2015). Deep coseismic slip of the 2008 Wenchuan earthquake inferred from joint inversion of fault stress changes and GPS surface displacements. *Journal of Geodynamics*, *87*, 1–12. https://doi.org/10.1016/j.jog.2015.03.001

Claypool, A. L., Klepeis, K. A., Dockrill, B., Clarke, G. L., Zwingmann, H., & Tulloch, A. (2002). Structure and kinematics of oblique continental convergence in northern Fiordland, New Zealand. *Tectonophysics*, *359*(3–4), 329–358. https://doi.org/10.1016/S0040-1951(02)00532-2

DeMets, C., Gordon, R. G., & Argus, D. F. (2010). Geologically current plate motions. *Geophysical Journal International*, *181*(1), 1–80. https://doi.org/10.1111/j.1365-246X.2009.04491.x

Dow, D. B., & Sukamto, R. (1984). Western Irian Jaya: The end-product of oblique plate convergence in the late Tertiary. *Tectonophysics*, *106*(1–2), 109–139. https://doi.org/10.1016/0040-1951(84)90224-5

Duquesnoy, T., Barrier, E., Kasser, M., Aurelio, M., Gaulon, R., Punongbayan, R. S., & Rangin, C. (1994). Detection of creep along the Philippine fault: First results of geodetic measurements on Leyte island, central Philippine. *Geophysical Research Letters*, *21*(11), 975–978. https://doi.org/10.1029/94GL00640

Fitch, T. J. (1972). Plate convergence, transcurrent faults, and internal deformation adjacent to Southeast Asia and the western Pacific. *Journal of Geophysical Research*, *77*(23), 4432–4460. https://doi.org/10.1029/JB077i023p04432

Hanks, T. H. (1977). Earthquake stress-drops, ambient tectonic stresses, and the stresses that drive plates. *Pure and Applied Geophysics*, *115*(1-2), 441–458. https://doi.org/10.1007/BF01637120

Huang, M.-H., Tung, H., Fielding, E., Huang, H.-H., Liang, C., Huang, C., & Hu, J.-C. (2016). Multiple fault slip triggered above the 2016 Mw 6.4 MeiNong earthquake in Taiwan. *Geophysical Research Letters*, *43*, 7459–7467. https://doi.org/10.1002/2016GL069351

Kreemer, C., Holt, W. E., Goes, S., & Govers, R. (2000). Active deformation in eastern Indonesia and the Philippines from GPS and seismicity data. *Journal of Geophysical Research*, *105*(B1), 663–680. https://doi.org/10.1029/1999JB900356

Kundu, B., Yadav, R. K., Bali, B. S., Chowdhury, S., & Gahalaut, V. K. (2014). Oblique convergence and slip partitioning in the NW Himalaya: Implications from GPS measurements. *Tectonics*, *33*, 2013–2024. https://doi.org/10.1002/2014TC003633

Lawson, C. L., & Hanson, R. J. (1974). *Solving least squares problems*. Englewood Cliffs, NJ: Prentice Hall.

Massonnet, D., Rossi, M., Carmona, C., Adragna, F., Peltzer, G., Feigl, K., & Rabaute, T. (1993). The displacement field of the Landers earthquake mapped by radar interferometry. *Nature*, *364*(6433), 138–142. https://doi.org/10.1038/364138a0

Maung, H. (1987). Transcurrent movement in the Burma-Andaman Sea region. *Geology*, *15*(10), 911–912. https://doi.org/10.1130/0091-7613(1987)15%3C911:TMITBS%3E2.0.CO;2

McCaffrey, R., Zwick, P. C., Bock, Y., Prawirodirdjo, L., Genrich, J. F., Stevens, C. W., et al. (2000). Strain partitioning during oblique plate convergence in northern Sumatra: Geodetic and seismologic constraints and numerical modeling. *Journal of Geophysical Research*, *105*(B12), 28,363–28,376. https://doi.org/10.1029/1999JB900362

Michel, R., Avouac, J.-P., & Taboury, J. (1999). Measuring ground displacements from SAR amplitude images: Application to the Landers Earthquake. *Geophysical Research Letters*, *26*(7), 875–878. https://doi.org/10.1029/1999GL900138

Okada, Y. (1985). Surface deformation to shear and tensile fault in a half-space. *Bulletin of the Seismological Society of America*, *75*(4), 1135–1154.

Pérez-Cáceres, I., Simancas, J. F., Poyatos, D. M., Azor, A., & González Lodeiro, F. (2015). Oblique collision and deformation partitioning in the SW Iberian Variscides. *Solid Earth*, *7*(3), 857–872. https://doi.org/10.5194/se-7-857-2016

Philippine Institute of Volcanology and Seismology (2017). Surface rupture of the 2017 M6.5 Leyte earthquake along the Philippine fault Leyte segment. Retrieved from http://www.phivolcs.dost.gov.ph/index.php?option=com_content&view=article&id=7652:surface-rupture-of-the-2017-m65-leyte-earthquake-along-the-philippine-fault-surigao-segment&catid=60:latest-news&Itemid=19

Prioul, R., Cornet, F. H., Dorbath, C., Dorbath, L., Ogena, M., & Ramos, E. (2000). An induced seismicity experiment across a creeping segment of the Philippine fault. *Journal of Geophysical Research*, *105*(B6), 13,595–13,612. https://doi.org/10.1029/2000JB900052

Rangin, C., Le Pichon, X., Mazzotti, S., Pubellier, M., Chamot-Rooke, N., Aurelio, M., et al. (1999). Plate convergences measured by GPS across the Sundaland/Philippine Sea Plate deformed boundary: The Philippines and eastern Indonesia. *Geophysical Journal International*, *139*(2), 296–316. https://doi.org/10.1046/j.1365-246x.1999.00969.x

Sandwell, D., Mellors, R., Tong, X., Wei, M., & Wessel, P. (2011). Open radar interferometry software for mapping surface deformation. *Eos, Transactions American Geophysical Union*, *92*(28), 234–235. https://doi.org/10.1029/2011EO280002

Taira, A., Sato, Y., & Hashimoto, M. (1983). The role of oblique subduction and strike-slip tectonics in the evolution of Japan. In T. Hilde & S. Uyeda (Eds.), *The Western Pacific – Indonesian Region*, *Geodynamic Series* (Vol. 11, pp. 303–316). Washington, DC: American Geophysical Union. https://doi.org/10.1029/GD011p0303

Walcott, R. I. (1998). Modes of oblique compression: Late Cenozoic tectonics of the south island of New Zealand. *Reviews of Geophysics*, *36*(1), 1–26. https://doi.org/10.1029/97RG03084

Wegmuller, U., & Werner, C. (1997). Gamma SAR processor and interferometry software. In *Proceedings of 3rd ERS Symposium, Space Service Environment* (Spec. Publ. 414, Vol. 3, pp. 1687–1692). ESA: Florence, Italy.

Welstead, S. T. (1999). *Fractal and wavelet image compression techniques*. Bellingham, Washington: SPIE Optical Engineering Press. https://doi.org/10.1117/3.353798

Wessel, P., & Smith, W. H. F. (1998). New, improved version of Generic Mapping Tools released. *Eos, Transactions American Geophysical Union*, *79*(47), 579. https://doi.org/10.1029/98EO00426

Yang, Y.-H., Chen, Q., Liu, G.-X., Chen, H. Q., Liu, L. Y., & Hu, J.-C. (2014). Correction of coseismic deformation field associated with Wenchuan earthquake with GPS observables and InSAR adjacent track smoothing and fault slip inversion [in Chinese]. *Chinese Journal of Geophysics-Chinese Edition*, *57*(5), 1462–1476. https://doi.org/10.6038/cjg20140511

Yang, Y. H., Chen, Q., Liu, G. X., Li, Z. L., Cheng, H. Q., & Liu, L. Y. (2013). SAR image coregistration using fringe definition detection. *Journal of Mountain Science*, *10*(5), 790–800. https://doi.org/10.1007/s11629-013-2536-5

Yang, Y.-H., Chen, Q., Xu, Q., Zhang, Y., Yong, Q., & Liu, G. (2017). Coseismic surface deformation of the 2014 Napa earthquake mapped by Sentinel-1A SAR and accuracy assessment with COSMO-SkyMed and GPS data as cross validation. *International Journal of Digital Earth*, *10*(12), 1197–1213. https://doi.org/10.1080/17538947.2017.1299806

Yang, Y.-H., Chen, Q., Xu, Q., Zhang, Y.-J., Luo, R., Hu, J.-C., et al. (2017). SAR ionosphere signal correction for deformation field of Wenchuan earthquake and extraction of fault surface rupture trace. *Chinese Journal of Geophysics-Chinese Edition*, *60*(8), 2948–2958. https://doi.org/10.6038/cjg20170804